JOURNAL OF MATERIALS SCIENCE 17 (1982) 2469–2480

Crack-front shape effects in the double torsion test

P. S. LEEVERS
Department of Mechanical Engineering, Imperial College of Science and Technology, London, UK

The conventional use of the double torsion test to measure the rate dependence of crack growth is here subjected to a critical re-examination. Following from a series of such tests on polyesters, this examination was motivated by misgivings on the role of crack front curvature in undermining the geometry-independence of the results. Working through a successful prediction of the crack shape from simple (but experimentally justified) geometric considerations, an analysis leads to a general relation describing the distortion of the measured fracture toughness versus crack speed characteristics in terms of a single, measurable crack shape factor.

1. Introduction

The work reported here originated in a series of double torsion (DT) tests on thermosetting polyesters. This type of test – whose development can be traced to work by Outwater and Murphy [1] and by Kies and Clark [2] – has since become a widely used method of investigating crack growth in rate-dependent systems. The rate dependence may arise from transport phenomena in an aggressive environment [3], from inherent visco-elasticity in the material itself [4], or from both [5], but it normally causes behaviour steady enough to permit a quasi-static analysis. Nevertheless, use of the test has been extended into regimes of unsteady, unstable behaviour such as "stick–slip" crack growth, notably in epoxies [6, 7], but also in polymer/environment systems [5]. Our own use of the test was focused on the interesting instabilities observed under some circumstances when using the DT method to evaluate fracture toughness (K_c) against crack velocity ($\dot{a}$) curves.

The attraction of the DT test lies in its apparent simplicity. It allows a displacement-controlled machine (such as the screw-driven Instron type) to be used to drive a crack through the specimen, at any desired constant speed, for a convenient distance (nearly 100 mm in our own tests). All of the readings normally required can be derived from the resulting load–displacement curve. The resistance, R, of the material to a propagating crack – expressed as strain-energy release rate, G_c, or fracture toughness, K_c – is then plotted as a function of the crack velocity as measured or (more commonly) as calculated from the cross-head speed and force, and the crack-length derivative of specimen compliance. This convenient and straightforward test is, unfortunately, marred by an intrinsic fault: the propagating crack front is markedly curved. As a result, the crack velocity as measured conventionally does not have any unambiguous physical interpretation as the basis for a unique material response, and the derived $K_c(\dot{a})$ or $G_c(\dot{a})$ curves do not represent geometry-independent material properties. The object of this paper is to derive a working analytical description of the DT crack-front shape, and to use it to remove this ambiguity.

The supporting arguments exhibit an emphasis on the geometry of *deformation* near the crack front, rather than on the material's response to any measure of the local *stress*. This viewpoint can be illuminating, even at a very basic, heuristic level. Previous analysis of crack-front shapes has generally incorporated, explicitly or otherwise, the assumption that K_c during propagation (and thus K at any subcritical load) is constant along them. That this is insufficient to locate the front is easily demonstrated by considering the stability of a small perturbation in it, perhaps a part-circular advance from an otherwise straight section.

0022–2461/82/092469–12$03.94/0

Whatever abstraction from the stock of available K solutions is chosen to represent this situation, it is clear that K at the tip of this "salient" will exceed the global value. Propagation will henceforward initiate at this point – a recipe for instability.

What has been overlooked here is that any crack front is very much a three-dimensional object. A finite opening displacement always exists near the tip of a propagating crack: the fracture surfaces sweep inwards towards the nominal (median) crack plane, meeting almost perpendicular to it. Because only on this line of intersection is any surface created, local advance of a small salient on it is coupled to distortion of the entire connected surface. Since (at least outside the immediate vicinity of the tip) this surface is the boundary of an elastic continuum, its constraint to a necessarily smooth and continuous geometry guarantees that of the crack front. Choosing a local co-ordinate system (x, y) in the crack plane, the front can be described by a function:

$$y = F(x, t),$$

whose partial derivatives with respect to x and to time t (denoted by a superior dot) exist everywhere along it.

Local crack advances which are spurious to changes in the geometry of the surrounding continuum thus annihilate rather than perpetuate themselves. This viewpoint can, under some circumstances, be followed a step further, and the actual local stress concentration due solely to the crack front deemed to have no effect on this geometry: the interaction is one-way, the front visualized as a purely geometric entity conforming passively to a pre-existing displacement field. It is not suggested that this approach, which yields a closed solution here, will always be equally successful. The criterion of its usefulness will generally be that elastic displacements are large (the specimen compliance high) relative to the crack size.

The DT specimen fulfils this requirement and, certainly, the search for a uniform-K crack profile has not supplied a closed solution: merely, as for its localized use above, a paradox. Using finite element analysis, it can be shown that the existence of such a profile is at least possible [8]; however, if K_c is a function of the local "radial" crack speed, K will then vary along it as it translates. The *a priori* assumption that this cannot be so leads to the conclusion that the DT crack shape depends directly on the K_c against crack speed function [9], but, ultimately, this argument predicts the profile for a rate-independent K_c to be a straight line. This contradicts the finite element solution and conflicts with results presented below. These results will thus be used both to illustrate the conventional DT analysis (and its overall predictive success), but also to motivate its ensuing modification.

It remains an article of faith here that the rate-dependence of fracture in any material is uniquely expressed in the variation of its crack resistance (the work irrecoverably absorbed in creating unit projected area of crack surface) with crack speed. Since any point on a moving crack front is an *event*, having no persistent identity, the definition of "crack speed" in general can be freely chosen on an *ad hoc* basis. However, the focus of interest here is a rate-dependence originating in processes very local to the crack tip, so that only a definition which expresses their rate in a co-ordinate-free way will suffice. This must be a scalar multiple (we choose unity) of the velocity $\dot{\xi}$ of the crack front along its local normal ξ in the material. Thus (Fig. 1):

$$\dot{\xi} = \dot{F} \sin \phi, \tag{1}$$

where

$$\sin \phi = \left[1 + \left(\frac{\partial F}{\partial x}\right)^2\right]^{-\frac{1}{2}}. \tag{2}$$

In quasi-two-dimensional geometries, such as the DT type, the front shape function F is usually collapsed into a vector, a, whose time derivative $\dot{a}$ (the "crack velocity") is readily yielded by analysis or observation: but some important information is lost in the process. Only for a *translated* crack shape $f(x)$:

$$F(x, t) = a + f(x), \tag{3}$$

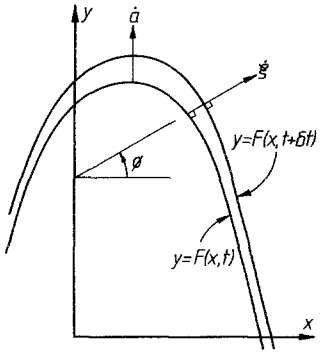

Figure 1 Propagation of a curved crack front.

are $\dot{F}$ and $\dot{a}$ the same, and only for a straight front orthogonal to a ($f = 0$, the true two-dimensional case) is $\dot{a}$ an invariant (scalar) measure of the fracture process rate.

2. Double torsion testing

2.1. The basic analysis

We can begin a more detailed examination of the DT test by presenting, for reference, its conventional analysis. The specimen geometry and its notation are shown in Fig. 2; the side grooves, a practical detail necessary to restrain the crack path to the centreline, are assumed sufficiently shallow to leave the torsional rigidity of each beam unaffected. There is assumed to be a constant angle of twist $d\theta/dy$ from the loading point ($y = 0$, $\theta = \theta_p$) to the crack tip ($y = a$, $\theta = \theta_t$), where θ is the rotation of each beam.

If this rotation remains small, it is linear with the applied moment M ([10], p. 309):

$$\frac{d\theta}{dy} = -\frac{2(1+\nu)}{E}\frac{1}{ZHB^3}M, \tag{4}$$

where

$$M = \frac{PD}{2},$$

and Z is a tabulated function of (H/B), tending to 1/3 as this ratio becomes large. E and ν are the elastic modulus and Poisson's ratio. Thus:

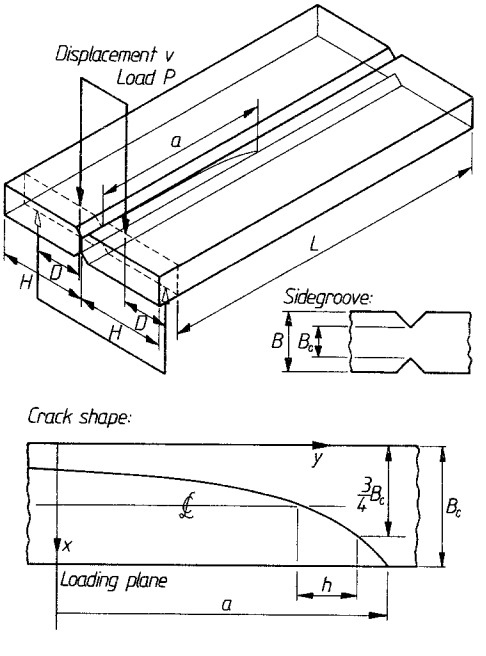

Figure 2 The double torsion test.

$$\frac{d\theta}{dy} = -\frac{(1+\nu)}{E}\frac{PD}{ZHB^3}. \tag{5}$$

At this point, it is usual to assume that both torsion beams are effectively built-in at the crack tip, but this is unnecessary. It is sufficient (and far more realistic) to assume the "ligament" $(L - a)$ to have a torsional compliance, $C_{\theta t}$, to to the moment transmitted by each beam, which is finite but independent of a. This implies that the deformation system in the ligament is localized at the beam roots. In practice, this root compliance seems to remain constant until the ligament is reduced to about H, rising rapidly thereafter.

Thus, for $(L - a) > H$, the beam root rotation is:

$$\theta_t = \frac{PD}{2}C_{\theta t}, \tag{6}$$

and that at the loading plane is:

$$\theta_p = \frac{PD}{2}C_{\theta t} + \frac{(1+\nu)}{E}\frac{PD}{ZHB^3}a. \tag{7}$$

Converting to a linear load-point compliance, $C \equiv v/P$, gives:

$$C = C_t + \frac{(1+\nu)}{E}\frac{D^2}{ZHB^3}a, \tag{8}$$

where $C_t \equiv \frac{1}{2}D^2C_{\theta t}$, and is therefore constant under the conditions already stated.

It is well known that for a small virtual extension of the crack, the elastic energy release rate will be:

$$G = \frac{P^2}{2}\frac{(dC/da)}{(dA/da)}, \tag{9}$$

where A is the area of fracture surface. For a straight crack front orthogonal to a, $(dA/da) = B_c$, and it can be assumed that all of the strain energy released during crack extension under a load P_c is immediately absorbed *uniformly* in the creation of fracture surface. This reveals the crack resistance R as:

$$R = G_c = \frac{P_c^2}{2B_c}\left(\frac{dC}{da}\right), \tag{10}$$

and, from Equation 8, the compliance derivative is seen to be independent of a:

$$\frac{dC}{da} = \frac{(1+\nu)}{E}\frac{D^2}{ZHB^3}, \tag{11}$$

so that:

$$G_c = \frac{P_c^2}{2B_c}\frac{(1+\nu)}{E}\frac{D^2}{ZHB^3}. \quad (12)$$

Conversion to a critical stress-intensity factor, the fracture toughness, K_c, can be accomplished through the equations:

$$K_c = [EG_c]^{\frac{1}{2}}, \quad (13a)$$

for plane stress, or

$$K_c = \left[\frac{EG_c}{(1-\nu^2)}\right]^{\frac{1}{2}}, \quad (13b)$$

for plane strain conditions.

Consider now the situation in which the load points are driven together at a constant speed $\dot{v}$, causing propagation of the crack along y at a velocity:

$$\dot{a} = \dot{v}\frac{da}{dv}. \quad (14)$$

Since $C \equiv v/P$:

$$\frac{dC}{da} = \frac{1}{P_c^2}\left[P_c\frac{dv}{da} - v\frac{dP_c}{da}\right], \quad (15)$$

so that:

$$\dot{a} = \dot{v}/\left(P_c\frac{dC}{da} + C\frac{dP_c}{da}\right). \quad (16)$$

For steady-state propagation of the crack, P_c is constant and Equation 16 reduces to:

$$\dot{a} = \dot{v}/\left(P_c\frac{dC}{da}\right). \quad (16a)$$

The conditions under which steady-state crack propagation will take place depend on the nature of the material's time dependence. If E and R (thus G_c) are monotonically increasing functions of (or are independent of) rate, Equations 12 and 16 show that stability is ensured, any change in P_c being self-correcting. Testing a series of specimens at different cross-head speeds, and using these equations and independent evaluations of E and ν, then allows toughness to be plotted as a function of crack velocity. If, however, toughness *decreases* with increasing rate, then P_c will fall as $\dot{a}$ increases which – as Equation 16 shows – will engender instability, and the technique becomes difficult or indefinite in use. In practice, modest inverse rate-dependence raises only minor problems.

2.2. Experimental details

The DT technique was used to derive K_c against crack-velocity curves for eight thermosetting polyester resins specially made and supplied by BP Chemicals Limited. Only illustrative, but representative, results from three of these will be quoted here: one orthophthalic resin, Cellobond A360/157, and two isophthalics, Cellobond A273/301 and A283/270. These were characterized by tests to establish the yield stress, p_y (in compression on barrel-shaped specimens, at three strain rates from 10^{-3} to $10^{-1}\,\mathrm{sec}^{-1}$) and by modulus measurements in three-point bending, also at three strain rates spanning two decades.

6 mm plates of each resin were cast between glass plates, machined into DT specimens with dimensions $H = 45$ mm and $B_c = 3$ mm (Fig. 2), and postcured/stress-relieved. These were tested in a locating jig (maintaining $D = 25$ mm) with an integral load cell, driven by an Instron frame at cross-head rates spanning the four decades or so available. Load, P, versus displacement, v, plots were recorded – with the aid of a transient recorder at high speeds. At low speeds, progress of the crack front was monitored by eye and recorded on the P/v plot. This information normally provided the compliance derivative, and a direct measurement of crack velocity for comparison with that calculated from Equation 16. Provided that the second term in the denominator was retained for cases in which load variation occurred as a result of variation in B_c, agreement was excellent – well within 5%. Some materials (A360/157, for example) would not sustain crack growth at speeds sufficiently low for this type of observation, and recourse to a less direct method of compliance calibration was necessary. This was to cut a progressively longer, straight-fronted notch down the crack plane with a hacksaw, and to construct a C against a curve from measurements after each finite extension. The results from these experimental compliance calibrations were applied to other tests on the same material by factoring them according to E at the relevant rate, thickness B as measured, and their weighting in dC/da as revealed by Equation 11.

Fig. 3 illustrates K_c against $\dot{a}$ curves for the three materials. Two of these, A360/157 and A273/301, showed stick–slip behaviour at low speeds. Indeed, A360/157 was so prone to crack arrest at speeds of less than $1\,\mathrm{mm\,sec}^{-1}$ that the subsequent jump usually broke the specimen, making testing very difficult; dubiously high initiation values are not quoted.

More relevant here is the instability of crack propagation shown by tests in regimes with a falling K_c against $\dot{a}$ characteristic. These were

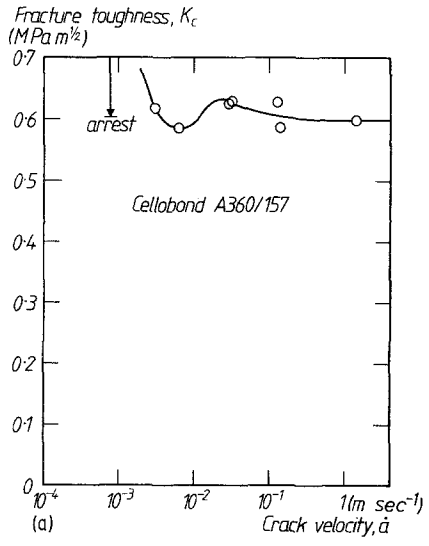

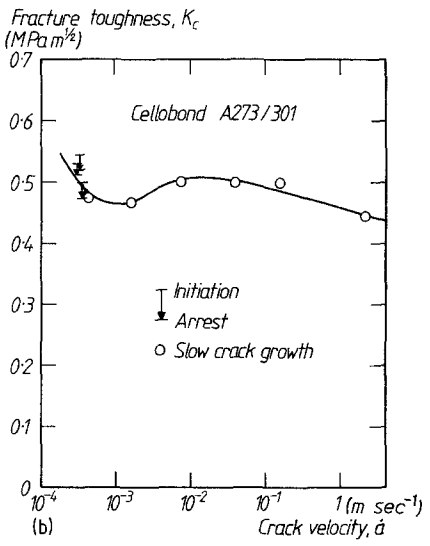

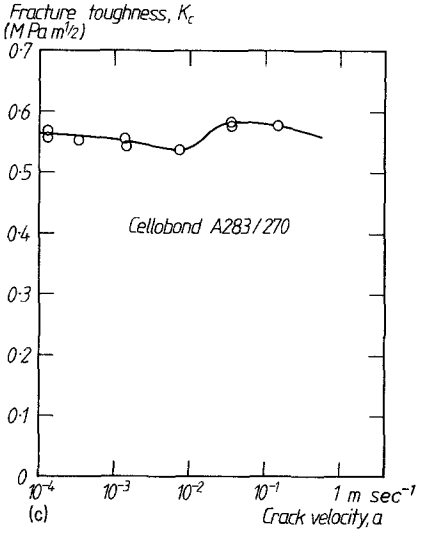

Figure 3 Fracture toughness as a function of crack velocity in DT tests: (a) Cellobond A360/157; (b) Cellobond A273/301; and (c) Cellobond A283/270.

easily identifiable (providing a lot of the extra information needed to plot smooth curves through the data points) by the tendency of the crack to propagate at two – sometimes more – distinct, alternate velocities, the overall velocity being their time average. This phenomenon was sometimes noticeable during testing as a regular jump of a millimetre or so, after perhaps five millimetres of growth at a uniform, lower rate: but it seldom registered significantly on the load/displacement chart. At higher rates, this instability caused a characteristic "unzipping" sound during fracture. Under other conditions, the two speeds were so similar as to make direct observation difficult, but, as for all cases of this type of behaviour, the exposed fracture surface showed a banded structure (Fig. 4) of alternating textures. Tests under conditions of K_c constant or rising with $\dot{a}$ always revealed uniform surfaces.

As well as increasing the resolution of data into a composite curve, this interesting phenomenon clearly marks many successive positions of the crack front. The best of these banded surfaces were metallized to aid observation, and photographed at a magnification of about 12. The photographs were assembled into lengths of up to 15 crack widths, and provided a rich source of data on the crack shape as it developed along the specimen.

2.3. Effects of crack-front curvature

Fig. 5 is a typical section from one of these composite surface micrographs; obviously, the straight crack front assumed by the conventional analysis is far from a realistic representation. The actual profile meets the lower surface at some angle less than 90°, and sweeps back to approach the upper surface asymptotically.

In essence, the effects of crack curvature on the overall deformation system will be those of the additional tractions exerted on what would have been the crack face, for $y < a$, if the front had been straight. These will exert a moment at any section which will resist that applied by the load, and will accumulate, causing the section moment to decay, from $y = 0$ to $y = a$. Thus,

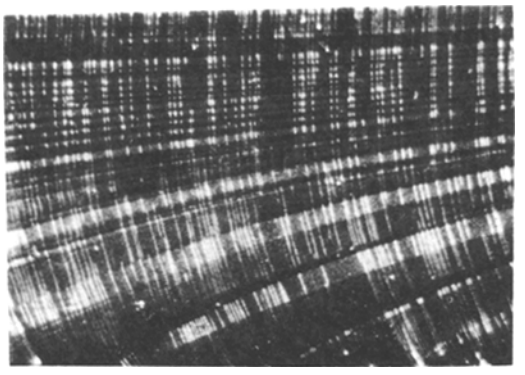

Figure 4 Bands of varying texture on fracture surface, indicating speed instabilities in a DT test. Crack velocity is to the left on lower surface.

from Equation 4, the angle of twist will also decay, reducing the apparent load point compliance C_t of the ligament. This effect on C_t should be observed by comparing results from the two calibration methods described in Section 2.2, using straight and curved fronts.

Fig. 6 shows C against a curves from a natural crack and from a saw-cut notch in A283/270, and Table I summarizes results from these and from another specimen in which a natural crack was driven at a different velocity. These have been corrected for rate and thickness variations: note the assumption that C_t, as well as the torsion beam compliance, varies as B^{-3}. The remaining differences become even less significant if it is noted that test 2 was generally more reliable, having been carried out at a slower cross-head speed, and having revealed a constant-P_c characteristic (unlike test 4, whose trace was slightly distorted by variation in B_c). It can be concluded that the two compliance calibration methods do not produce significantly different results.

3. Further analysis of the DT test

3.1. Crack shape

Thus, the reduction in C_t due to crack-front curvature is insignificant, compared to the total compliance at normal crack lengths. This strongly suggests that the torsional stiffness at any section is primarily determined by the geometrical properties of that section, so that the angle of twist remains constant along the crack length and determines the beam separation at the crack plane. One further assumption facilitates crack-shape prediction: that this separation is a constant, δ_f, along the front. The underlying hypothesis, that the near-tip section geometry and deformation in elastic response to its associated stress concentration remains constant, can be tested against reality by comparing the actual crack shape and with that predicted (as at the end of this section), and by comparing evaluations of δ_f with estimates of the critical crack tip COD, δ_c (as in the next section).

Fig. 7 shows the assumed geometry of the specimen's deformation, and that of the crack plane. A fulcrum point, $y = a + SB_c$, is introduced, at which the rotation θ extrapolates to

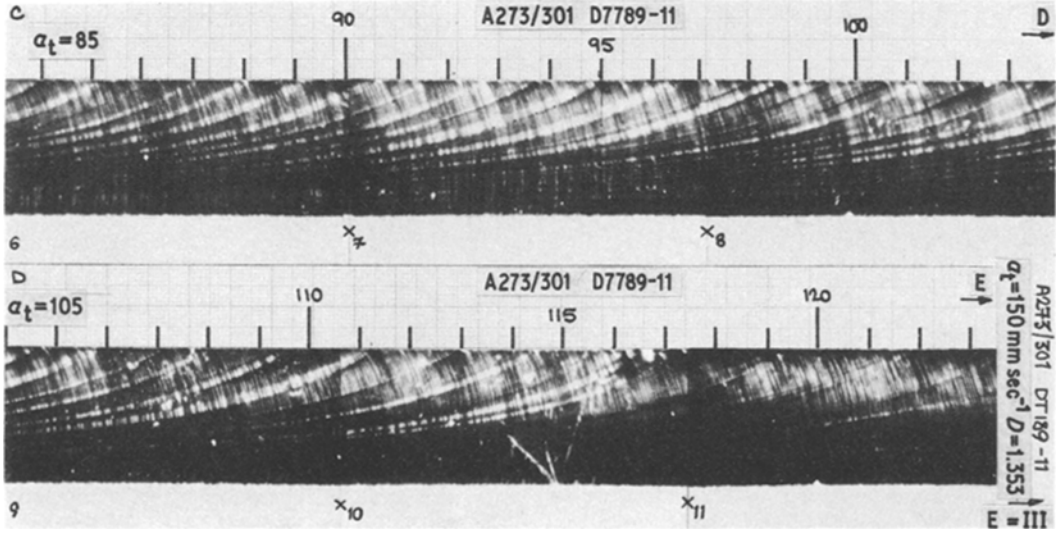

Figure 5 Reduction from a typical composite DT fracture surface micrograph, showing many successive crack-front positions.

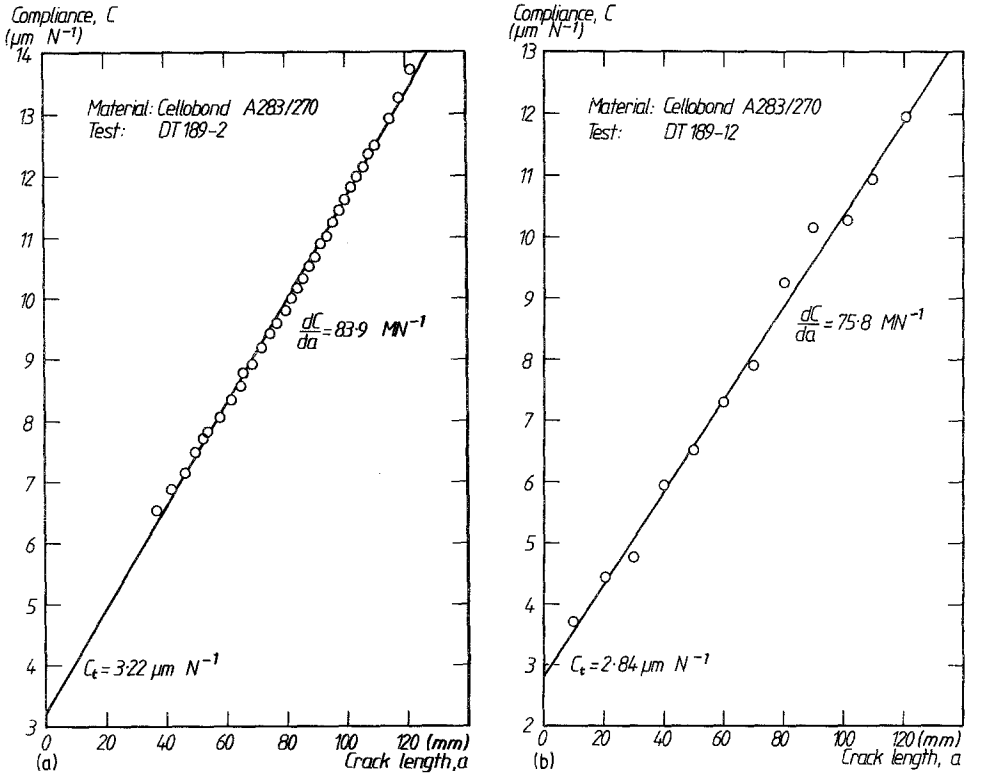

Figure 6 Compliance against crack-tip position in a DT specimen of Cellobond A283/270: (a) natural (curved) crack front; (b) artificial straight-fronted notch.

zero. Thus:

$$\theta(y) = \left(\frac{a + SB_c - y}{a + SB_c}\right)\theta_p = \left(1 - \frac{y}{a + SB_c}\right)\frac{v}{D}. \quad (17)$$

Now, let displacements in the crack plane be given by a simple rotation about a hinge half-way from the crack front to the upper edge of the crack plane (Fig. 7b). The separation δ is then:

$$\delta(x,y) = 2\theta(y)\left(x - \frac{b}{2}\right) = \left(x - \frac{b}{2}\right)\left[1 - \frac{y}{(a + SB_c)}\right]\frac{2v}{D}. \quad (18)$$

On the crack front F, $\delta = \delta_f$, and so:

$$\delta_f = \frac{vb}{D}\left[1 - \frac{F(x)}{(a + SB_c)}\right], \quad (19)$$

while on the lower surface ($x = b = B_c, F(x) = a$):

$$\delta_f = \frac{vB_c}{D}\left[1 - \frac{a}{(a + SB_c)}\right]. \quad (20)$$

Eliminating $(a + SB_c)$ from Equations 19 and 20 gives the crack shape:

$$F(x) = \frac{aB_c}{x}\left[\frac{vx - D\delta_f}{vB_c - D\delta_f}\right]. \quad (21)$$

Normalizing co-ordinates against the crack path width, we put:

TABLE I C and dC/da for natural cracks (NC) and a straight saw-cut crack (SC) in A283/270 DT specimens

Specimen number	Method	C_t ($\mu m\ N^{-1}$)	dC/da (MN^{-1})	Cross-head speed, $\dot{v}$ ($mm\ min^{-1}$)	Thickness, B (mm)	Modulus, E (GPa)	$(EB^3)\,C_t$ (mm^2)	$(EB^3)\,(dC/da)$ (mm)
DT189-2	NC	3.22	83.9	0.05	5.87	3.59	2340	60.9
DT189-4	NC	3.13	75.5	0.25	5.97	3.63	2420	58.3
DT189-12	SC	2.84	75.8	0.5	6.01	3.70	2280	60.9

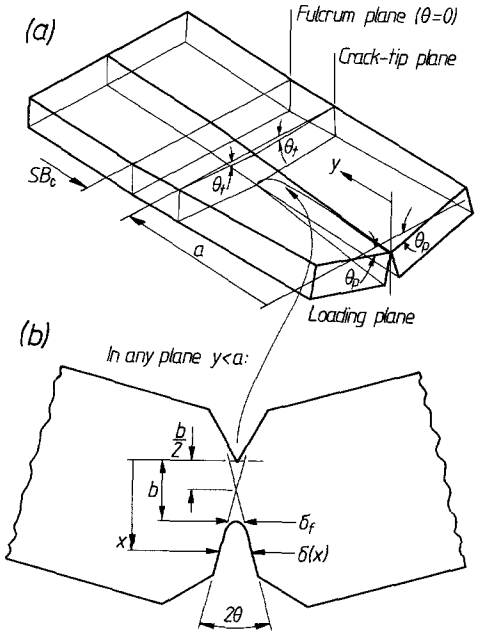

Figure 7 Deformation of (a) the DT specimen, and (b) its crack plane.

$$F^* \equiv \frac{a - F(x)}{B_c}, \tag{22}$$

$$x^* \equiv \frac{x}{B_c}, \tag{23}$$

and

$$\Delta \equiv \frac{\delta_f D}{B_c^2}, \tag{24}$$

and obtain:

$$F^*(x^*) = \frac{\Delta a[(1/x^*) - 1]}{(v - \Delta B_c)}. \tag{25}$$

Note that, as would be expected, the crack front never intersects the upper surface of its nominal path; at $y = 0$:

$$x_p^* = \frac{\Delta B_c}{v}. \tag{26}$$

Now, from Equation 2,

$$\sin\phi = \frac{(v - \Delta B_c)x^{*2}}{[\Delta^2 a^2 + (v - \Delta B_c)^2 x^{*4}]^{1/2}}, \tag{27}$$

and the crack velocity at a given x^* is, from Equation 22:

$$\dot{F}(x^*) = \dot{a} - B_c \dot{F}^*(x^*), \tag{28}$$

which, from Equation 25, becomes:

$$\dot{F}(x^*) = \left[(vx^* - \Delta B_c)\dot{a} + \frac{\Delta B_c(1 - x^*)}{(v - \Delta B_c)} a\dot{v}\right] \Big/ x^*(v - \Delta B_c). \tag{29}$$

The crack speed is therefore, from Equation 1:

$$\dot{\xi} = x^* \left[(vx^* - \Delta B_c)\dot{a} + \frac{\Delta B_c(1 - x^*)}{(v - \Delta B_c)} a\dot{v}\right] \Big/ [(v - \Delta B_c)^2 x^{*4} + a^2\Delta^2]^{\frac{1}{2}}. \tag{30}$$

Clearly, it is worth looking for a way to simplify these expressions. This can be found in the demonstrated success of the "simple" theory (assuming a straight crack front) in predicting the crack-length derivative of compliance, its independence of crack length over the central half or so of its path, and the consequent constant velocity of a crack driven by steady cross-head displacement. The revised theory must be consistent with these observations.

Rearranging Equation 20, we obtain:

$$v = \left[\frac{a}{S} + B_c\right]\Delta. \tag{31}$$

Only if S is constant can this expression be reconciled with Equation 16, which successfully predicts the observed proportionality of $\dot{a}$ and $\dot{v}$. With this assumption, Equation 31 differentiates to:

$$\dot{v} = \frac{\Delta\dot{a}}{S}, \tag{32}$$

and things get much simpler. Substituting Equation 31 into Equation 27 yields:

$$\sin\phi = \frac{x^{*2}}{(S^2 + x^{*4})^{1/2}}, \tag{33}$$

illustrating that the crack shape is independent of a under these circumstances, simply translating along the specimen in the wake of the advancing tip. From Equations 25 and 31, this shape is:

$$F^* = S\left(\frac{1}{x^*} - 1\right), \tag{34}$$

and its intersection point at the loading plane is:

$$x_p^* = \frac{S}{[S + (a/B_c)]}. \tag{35}$$

S is now revealed as a single scaling parameter characteristic of the particular test – a "crack-shape factor". Although for a given cross-head displacement and crack length an infinite number

of constant δ_f contours exist, S replaces δ_f, and a measure of the beam torsion, in fixing one of them. Its independence of crack length is a result of the constancy of fracture load and of the beam root compliance C_t (it is related to their product), since together these ensure that the entire deformation system translates unchanged along the specimen. The issue of the physical interpretation of δ_f will be returned to in the next section.

S is easily measured from arrest marks or banding on the fracture surface; some latitude exists in choosing a method for doing so. Equation 34 shows that the crack front intersects the crack plane centreline ($x^* = \frac{1}{2}$) at $F^* = S$, so that the crack front lags its tip by SB_c at this point (Fig. 2). Several reasons make this apparently obvious method by measuring S unsatisfactory in practice. Plane stress effects near the specimen boundary sometimes obscure the surface markings, and may affect the material separation mechanics. Furthermore, the assumption underlying the analysis – that the angle of twist in the torsion arms is unaffected by tractions acting in the crack plane – is progressively less realistic as the tip is approached. The evaluation technique was adopted to measure the axial (y) distance, h, between the half-width and three-quarters-width points on the front; since:

$$F^*(x^* = 0.5) - F^*(x^* = 0.75) = \tfrac{2}{3}S,$$

this leads to:

$$S = 1.5h/B_c. \qquad (36)$$

Fig. 8 shows S as a function of crack-tip position as propagation progresses for two materials, A360/157 and A273/301, showing, respectively, unusually high and fairly typical average values. In each case, S varies little over the central region of the path, in line with the constant crack velocity observed. For shorter cracks S is lower, for longer ones higher. Probably the most interesting feature of these measurements is that, particularly for A360/157, S values for transitions into and out of bands of a particular surface texture are consistently different. The possible reasons for this will be returned to in the next section.

Fig. 9 shows how the crack shapes measured from two tests, normalized against S, compare with that predicted by Equation 34. While for A273/301, with a lower S value, agreement is excellent, it is not so good for A360/157. However, substantial divergence from the predicted shape is restricted to a region very close to the tip; otherwise, a simple axial shift brings close agreement. This shift has no other significant effects, since the response of the specimen to crack translation is already established; but its necessity emphasizes the importance of evaluating S from the crack shape well behind the tip.

3.2. Deformation near the crack front

What does S really mean in terms of events near the crack front? Some attempt at answering this can be made by comparing δ_f (a COD value

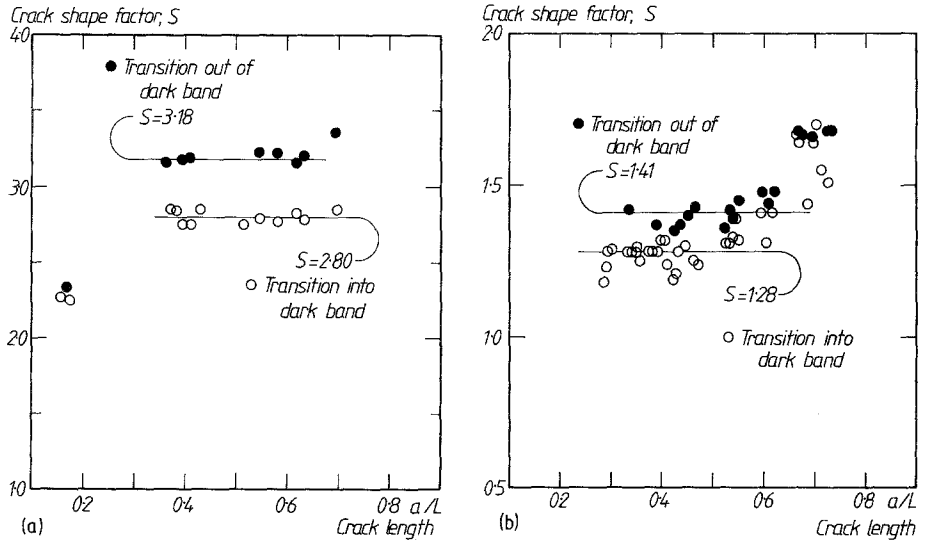

Figure 8 Variation of crack-shape factor S with crack extension: (a) $\dot{a} = 140$ mm sec^{-1} in A360/157; and (b) $\dot{a} = 7.3$ mm sec^{-1} in A273/301.

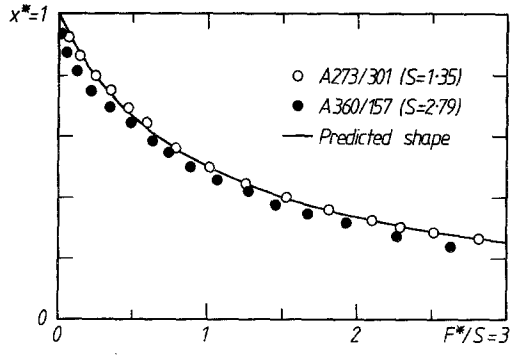

Figure 9 Predicted and observed crack shapes for the two DT tests of Fig. 8.

extrapolated from elastic deformations of the surrounding continuum and measured via S) with the critical COD δ_c (a material parameter representing the scale of plastic deformation at the crack front). Since measurements of crack velocity give values close to those predicted from Equation 16a, the clusters of constants in Equations 16a and 32 can be equated to give:

$$\delta_f = \frac{SB_c^2 P_c}{D} \frac{dC}{da}. \quad (37)$$

All the quantities on the right-hand side are readily accessible from DT tests. For the particular tests under examination here, the fracture load remained substantially constant, and values resulting from the S value shown in Fig. 8 are 2.3 and 2.8 μm for A273/301, and 3.8 and 4.4 μm for A360/157.

The critical COD values can be estimated from the Dugdale model as:

$$\delta_c = \frac{K_c^2}{Ep_y}, \quad (38)$$

although, for two reasons in particular, the estimate is unlikely to be an accurate one. Firstly, the model is only strictly applicable to co-linear plane stress plastic zones, or to crazes: neither of which is relevant here. Secondly, these materials are rate-sensitive, and the relevant rates for p_y are experimentally inaccessible: typically 1500 sec^{-1}. Using data for the highest rates tested yields values for δ_c of 0.7 μm in A360/157 and 0.4 μm in A273/301. Thus, δ_f is several times larger than δ_c, the difference reflecting the concentrated local *elastic* displacement field at the crack front. Nevertheless, this characteristic size of the crack front, which determines the position at which it fits into the overall deformation field, is of the same order as that of the process zone. Indeed, if the process were predominantly one of slip along angled bands, it would be feasible for changes in a process dimension to be reflected in changes in δ_f. For these materials, whose K_c value (and hence the scale of near-tip elastic displacements) is substantially independent of crack velocity, there is some tenuous evidence for this.

It has already been demonstrated that S can change abruptly by around 20% as the crack speed switches, while the fracture load hardly changes perceptibly. Thus, for small crack jumps, K_c remains substantially constant and, with it, the elastic part of the crack-front deformation field. The irreversible part characterized by δ_c, however, *does* change: this is revealed by the transition of surface texture in a banded formation (Fig. 4). Nevertheless, the absolute changes in δ_f (0.6 μm for A360/157 and 0.5 μm for A273/301) are of the same order as δ_c, making it likely that there is an elastic component to them. This may be possible within a few microns of the crack tip (even while K_c, essentially a macroscopic parameter, remains constant) if the change in process geometry is sufficiently drastic – from co-linear crazing to angled slip, to quote an extreme example. This whole area promises to be an interesting one for further investigation.

For the time being, S need only be regarded as a measurable characteristic of a particular DT test. The next section will demonstrate that it may still be an essential element in interpreting K_c or G_c against $\dot{a}$ data as a material characteristic.

3.3. Crack speed and apparent fracture toughness

For a translating crack which is curved, the measured $G_c(\dot{a})$ characteristic will not generally be the true $R(\dot{\xi})$ characteristic [11]: the released strain energy will be absorbed non-uniformly along the front, *none* of which necessarily advances at the measured translation velocity $\dot{a}$. An energy-balance argument leads straightforwardly to:

$$G_c(\dot{a}) = \int_{x_p^*}^{1} R[\dot{\xi}(\dot{a}, x^*)]\, dx^*, \quad (39)$$

and, using the present one-parameter description of the DT crack shape, closed-form solutions for the discrepancy are easily derived.

Since the crack profile is translated, $\dot{F} = \dot{a}$, and Equations 1 and 33 yield the crack-speed profile:

$$\dot{\xi} = \frac{\dot{a}x^{*2}}{(S^2 + x^{*4})^{1/2}}. \quad (40)$$

Fig. 10 illustrates this profile for the two materials examined, on a logarithmic scale to correspond to the $K_c(\dot{a})$ data. For A360/157, less than half of the surface area is exposed at even a tenth of the nominal rate. Substituting Equations 40 and 35 into Equation 39 gives:

$$G_c = \int_{S/(S+a/B_c)}^{1} R[(\dot{a}x^{*2})/(S^2 + x^{*4})^{1/2}]\, dx^*. \quad (41)$$

This integration is not particularly straightforward in general, but can be reviewed qualitatively for two simple cases.

For a non-time-dependent characteristic:

$$R = R_0, \quad (42)$$

a constant. Thus, the apparent toughness is:

$$G_c = R_0 \frac{a}{(SB_c + a)}, \quad (43)$$

which will be negligibly in error if the crack is sufficiently long. It was found experimentally, however, that values for SB_c of 8 mm were sometimes observed, yielding a 10% underestimate for G_c (5% for K_c) over the central region of crack length.

A common form of R characteristic for polymers (e.g. PMMA [4]) is:

$$R(\dot{\xi}) = R_0 \dot{\xi}^n, \quad (44)$$

where, usually, $n > 0$. The apparent characteristic from DT tests then becomes:

$$G_c = R_0 \dot{a}^n \int_{S/(S+a/B_c)}^{1} x^{*2n}/(S^2 + x^{*4})^{n/2}\, dx^*, \quad (45)$$

compounding the downward ($n > 0$) shift to a total constant factor of:

$$\frac{G_c}{R} = \int_{S/(S+a/B_c)}^{1} x^{*2n}/(S^2 + x^{*4})^{n/2}\, dx^*. \quad (46)$$

This expression was evaluated by numerical quadrature, and results for values of n typical of polymers are plotted in Fig. 11. Drastic as this correction may be for large values of n, it is at least easy to apply if S can be measured, and if the measured characteristic approximates to one of the simple forms (Equations 42 or 44). More complicated forms of rate dependency, such as those suggested by the measured characteristics in Fig. 3, present severe difficulties. Definition is lost, a downward shift is introduced, and peaks or notches are shifted to the right on the crack-speed axis.

4. Conclusions

(1) "Crack velocity" is a diffuse concept which can be fairly freely defined *ad hoc*. For use as a basis on which to plot the rate dependence of fracture toughness, however, the only rational

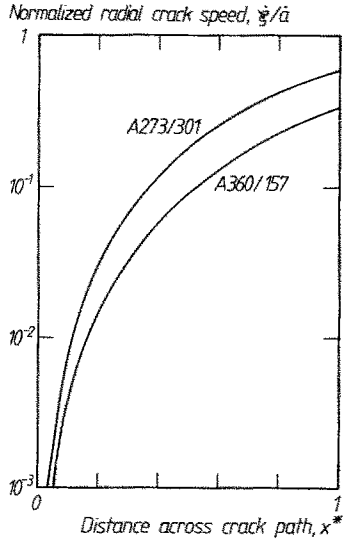

Figure 10 Calculated crack speed across the crack path in the two tests of Fig. 8.

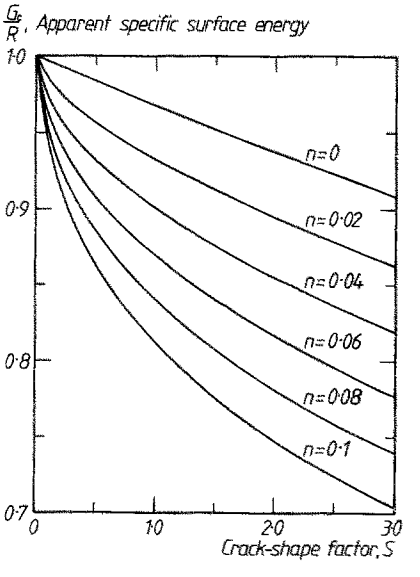

Figure 11 Effect of crack shape on DT test evaluation of G_c, for materials with a power-law (exponent n) rate dependence.

definition is as the radial speed of the front, that is, the speed of its point of intersection with a plane in the material instantaneously normal to it.

(2) The crack front propagated in a double torsion specimen is always markedly curved. Although the shape is preserved and merely translates axially, the local radial crack speed varies along it, casting doubt on the ability of the test to reveal a true fracture toughness against crack speed characteristic.

(3) Because the DT specimen is highly compliant, the crack-front shape can be quite accurately located by extrapolating the overall deformation system inwards to a point at which a particular, constant crack-surface displacement, δ_f, is implied. Full analysis yields a working prediction for the resultant crack shape.

(4) This shape is fixed by a single parameter, the "crack-shape factor" S, which can often be measured easily from fracture-surface markings. Using this, and other readily accessible test results, δ_f can be calculted.

(5) Results from tests on polyesters indicate that δ_f cannot be identified with a "critical COD", δ_c: it is several times larger, the excess representing an elastic displacement due to the local crack-front stress intensity, as measured by the factor K.

(6) The implication that a constant K criterion seems to govern the crack-front location is not really significant, since for these materials, K_c varies little with crack speed anyway. On the other hand, there is some tenuous experimental evidence (based on observations of surface roughness) that changes in δ_c also exert an influence on the crack-shape factor. Confirmation is contingent on more direct measurement of δ_c.

(7) From the predicted crack shape, an expression is derived which describes how the true toughness against crack-speed characteristic is modified as it is revealed by DT testing. The general effect is an underestimate; the upward-sloping exponential characteristics typical of polymers are further depressed, and local peaks and troughs are shifted to the right along the crack-speed axis.

Acknowledgements

The work reported here was supported by a grant from the Science and Engineering Research Council (Polymer Engineering Directorate), and by the provision of material and technical assistance from BP Chemicals Limited. The author would also like to thank Professor J. G. Williams and Dr Y. W. Mai for useful and stimulating discussions.

References

1. J. O. OUTWATER and M. C. MURPHY, *J. Adhesion* 2 (1970) 242.
2. J. A. KIES and A. B. J. CLARK, "Proceedings of the 2nd International Conference on Fracture" (Chapman and Hall, London, 1969) pp. 483–91.
3. A. G. EVANS, *J. Mater. Sci.* 7 (1972) 1137.
4. G. P. MARSHALL, L. H. COUTTS and J. G. WILLIAMS, *ibid.* 9 (1974) 1409.
5. M. I. HAKEEM and M. G. PHILLIPS, *ibid.* **14** (1979) 2901.
6. S. YAMINI and R. J. YOUNG, *ibid.* **14** (1979) 1609.
7. J. M. SCOTT, G. M. WELLS and D. C. PHILLIPS, *ibid.* **15** (1980) 1436.
8. G. G. TRANTINA, *J. Amer. Ceram. Soc.* **60** (1977) 338.
9. A. V. VIRKAR and R. S. GORDON, *ibid.* **58** (1975) 536.
10. S. P. TIMOSHENKO and J. N. GOODIER, "Theory of Elasticity", 3rd edn. (McGraw-Hill, New York, 1970).
11. J-C. POLLET and S. J. BURNS, *J. Amer. Ceram. Soc.* **62** (1979) 426.

Received 24 November 1981
and accepted 10 February 1982